Characterization of Layer Number and Crystal Anisotropy of CVD Grown $PdSe_2$ by Second Harmonic Generation and Low frequency Raman Spectroscopy

Hui-Yu Cheng[1*], Li-Syuan Lu[1], Yu-Ming Chang[2], and Wen-Hao Chang[1]

[1]*Department of Electrophysics, National Chiao Tung University, Hsinchu, Taiwan*

[2] *Center for Condensed Matter Sciences, National Taiwan University, Taipei, Taiwan*

* presenting author: Hui-Yu Cheng, email:cabin610082@gmail.com

Abstract

Two-dimensional (2D) $PdSe_2$ crystal is a member of 2D transition metal dichalcogenides, featuring a unique puckered pentagonal structure with in-plane anisotropy. $PdSe_2$ is theoretically predicted to exhibit a widely tunable bandgap varying from zero (bulk) to ~1.3 eV (monolayer). The strongly layer-number-dependent electronic and optical properties of $PdSe_2$ have attracted much attention because of its potential device applications. Here we demonstrate that the layer number and crystal anisotropy of 2D $PdSe_2$ can be identified by polarization-resolved low-frequency (LF) Raman spectroscopy and second harmonic generation (SHG). The strong interlayer interaction in 2D $PdSe_2$ is revealed by the layer-dependent Raman peaks, which can be well described by the conventional linear chain model corrected by a minor interlayer restoring forces. The layer number can be further confirmed by SHG imaging, where a strong (nearly vanished) SHG signal can be observed in even-layer (odd-layer) $PdSe_2$ crystals with a non-centrosymmetric (centrosymmetric) structure. Polarization-resolved Raman and SHG measurements also reveal in-plane anisotropy, which is consistent with the crystallographic axes determined by transmission electron microscopy. This work demonstrates that LF Raman spectroscopy and SHG are useful noninvasive methods for characterizing the layer number and crystallographic axes of 2D $PdSe_2$ crystals.

Sample Description

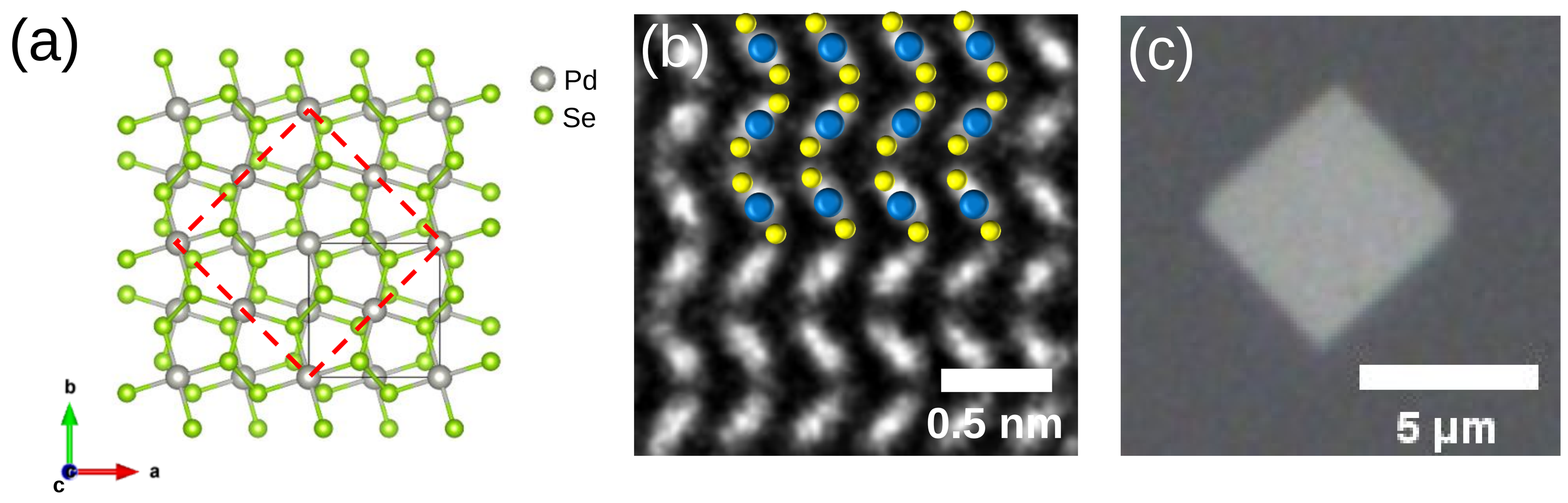

Figure 1. (a) Top view of the crystal structure of 2-layer (2L) $PdSe_2$ showing a puckered pentagonal configuration. (b) Atomic resolution structure of 2L $PdSe_2$ crystal revealed by TEM image. Inset showed atomic model of the corresponding TEM image. (c) Optical image (OM) of CVD grown $PdSe_2$ flake on sapphire substrate.

Characterization of Layer Number

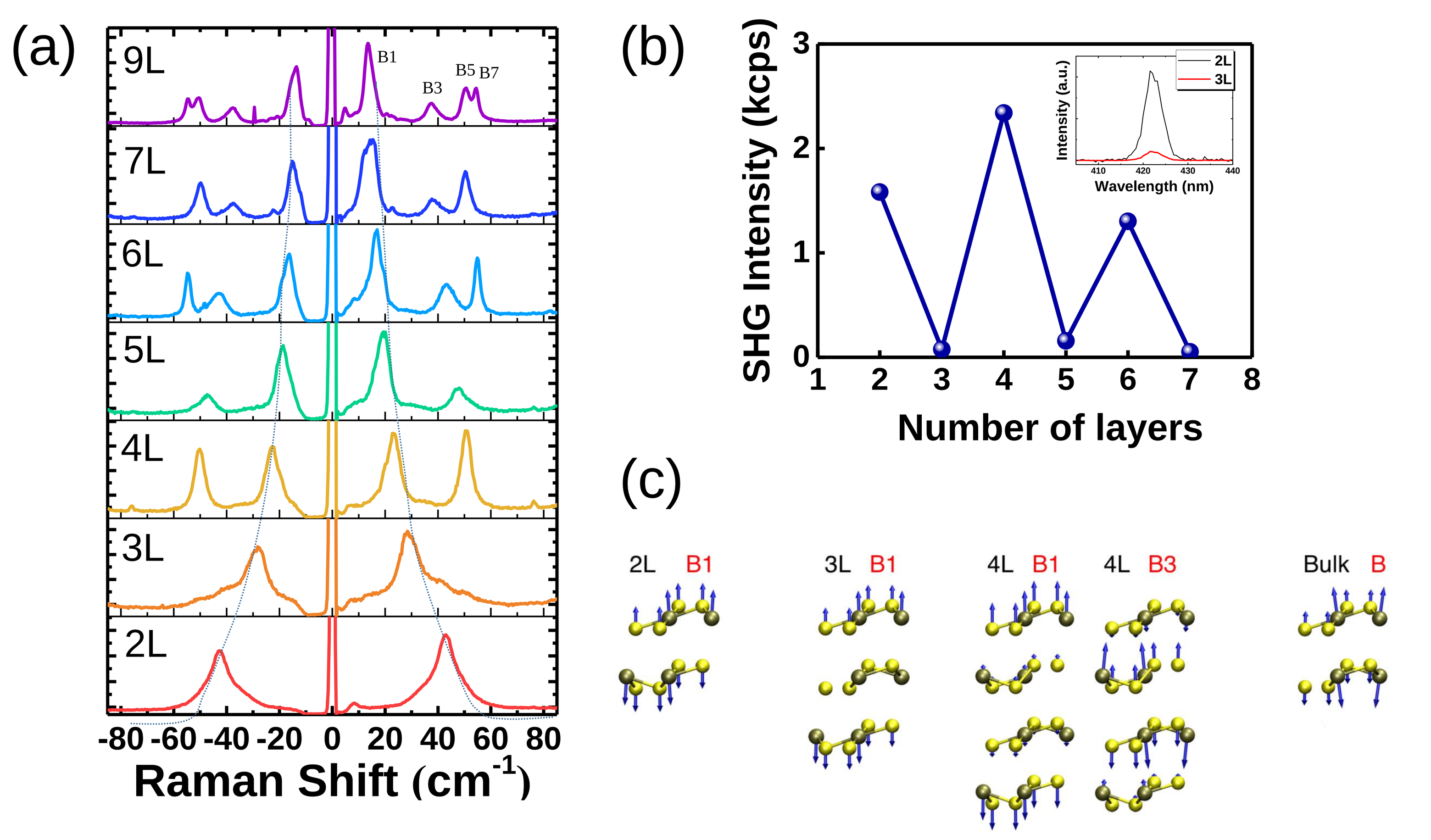

Figure 2. (a) Stokes and anti-Stokes LF Raman spectra for 2–9 layers of $PdSe_2$ measured in co-polarization configuration. The dotted lines show the evolution of the Raman shift for B1 breathing mode with the number of layers. Raman shifts of the breathing mode peaks for odd branches, B1–B7, versus the number of PdSe2 layers. (b) Layer dependence of the SHG intensity which is normalized at a SHG energy of 1.55 eV. The dependence of the SHG intensity oscillated with layer number in $PdSe_2$ crystal. (c) Vibrational patterns for 2L (B1); 3L (B1); 4L (B1, B3); and bulk (B) modes of $PdSe_2$.

Raman Selection Rule for $PdSe_2$

Raman tensor $\tilde{R}(A_g) = \begin{pmatrix} a & \cdot & \cdot \\ \cdot & b & \cdot \\ \cdot & \cdot & c \end{pmatrix}$

Raman intensity $I \propto |e_i \cdot \tilde{R} \cdot e_s|^2 = \left| (\cos\varphi, \sin\varphi, 0) \;\; \tilde{R} \begin{pmatrix} \cos\gamma \\ \sin\gamma \\ 0 \end{pmatrix} \right|^2$

(Incident light e_i; Scattered light e_s)

⇨ $I(A_g) \propto |a^2 \cdot \cos\varphi\cos\gamma + b^2 \cdot \sin\varphi\sin\gamma|^2$

co-polarization: $\varphi = \gamma$

⇨ $I(A_g) \propto |a^2 \cdot \cos^2\varphi + b^2 \cdot \sin^2\varphi|^2$

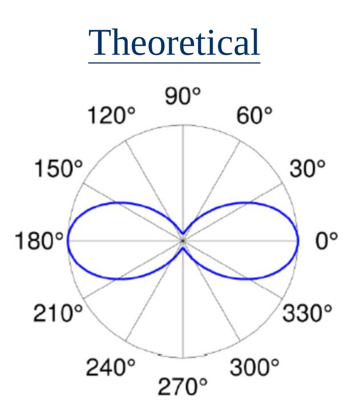

Second Harmonic Generation of $PdSe_2$

The symmetry of even-layer $PdSe_2$ belongs to point group C_{2v} (mm2). For symmetry axis along the b-axis, the second-order nonlinear susceptibility tensor can be written as:

$$\overleftrightarrow{\chi}^{(2)} = \begin{pmatrix} 0 & 0 & 0 & 0 & 0 & d_{16} \\ d_{21} & d_{22} & d_{23} & 0 & 0 & 0 \\ 0 & 0 & 0 & d_{34} & 0 & 0 \end{pmatrix}$$

SHG intensity $I_{2\omega} \sim \left|\hat{\mathbf{e}}_{2\omega} \cdot \overleftrightarrow{\chi}^{(2)} : \hat{\mathbf{e}}_{\omega}\hat{\mathbf{e}}_{\omega}\right|^2 I_{\omega}^2$

co-polarization:

⇨ $I_{\parallel} = \varepsilon_0{}^2 E_0^4 |A \cdot \sin\varphi + B \cdot \sin 3\varphi|^2$

cross-polarization:

⇨ $I_{\perp} = \varepsilon_0{}^2 E_0^4 |C \cdot \cos\varphi + D \cdot \cos 3\varphi|^2$

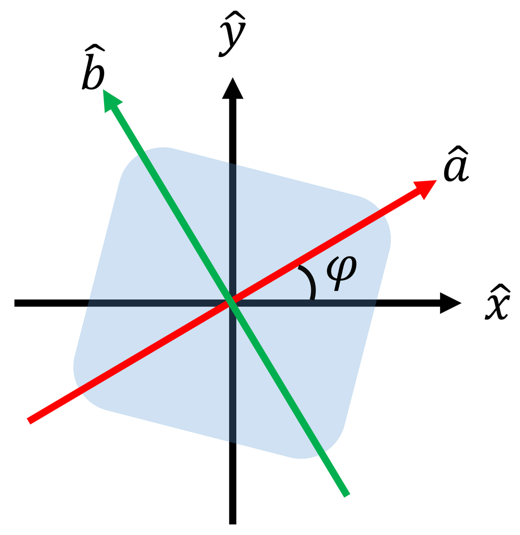

$$A = \left(\tfrac{1}{2}d_{16} + \tfrac{1}{4}d_{21} + \tfrac{3}{4}d_{22}\right) ; \; B = \left(\tfrac{1}{2}d_{16} + \tfrac{1}{4}d_{21} - \tfrac{1}{4}d_{22}\right)$$

$$C = \left(\tfrac{1}{2}d_{16} - \tfrac{3}{4}d_{21} - \tfrac{1}{4}d_{22}\right) ; \; D = \left(-\tfrac{1}{2}d_{16} - \tfrac{1}{4}d_{21} + \tfrac{1}{4}d_{22}\right)$$

Azimuthal Dependent Raman and SHG

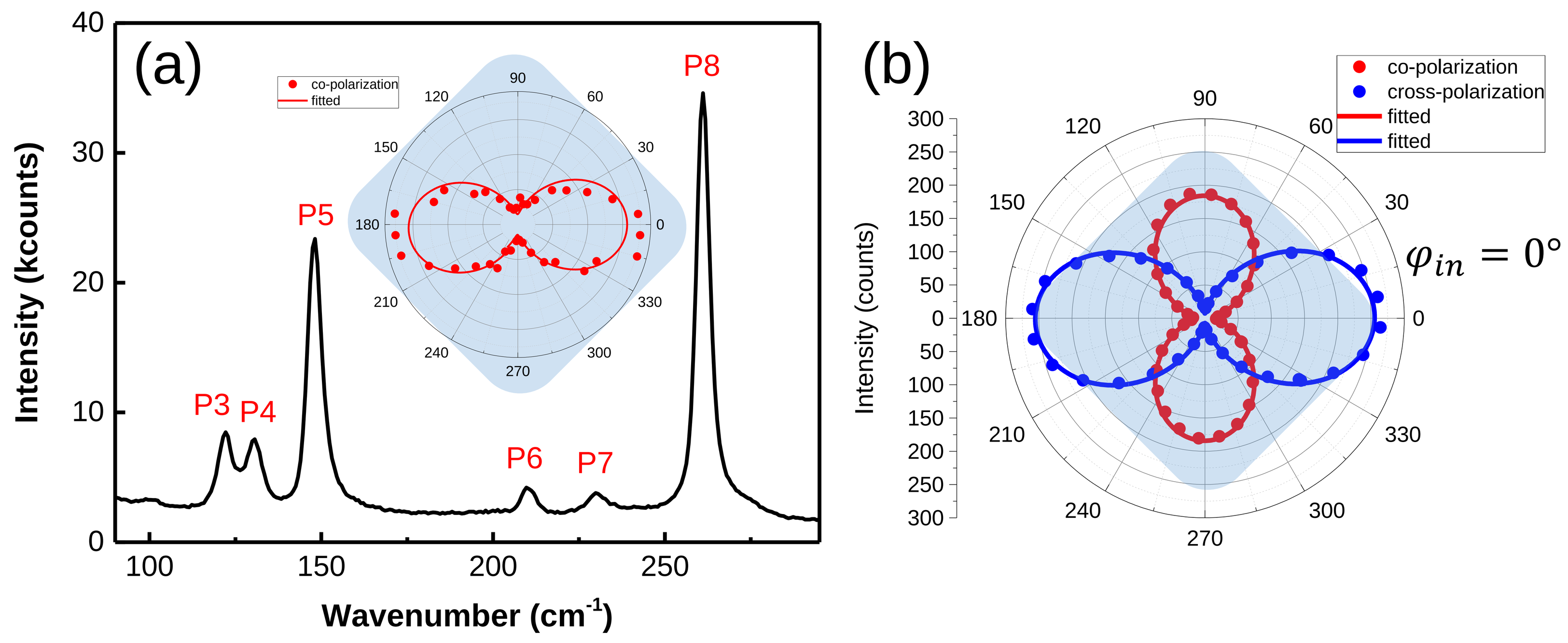

Figure 3. (a) Raman spectrum of 2L $PdSe_2$ measured in co-polarization configuration. Inset shows experimental (dots) and fit (curve) polar plots of P5 peak intensity versus φ. (b) Polar plot of the SHG intensity from 2L $PdSe_2$ as a function of φ. The SHG radiation components detected in co-(red) and cross-(blue) polarization configuration. The experimental data (dots) are well fitted by the theoretical analysis described above. Experimentally we set the input and output polarization configuration, then rotated the sample to obtain azimuthal angle dependent Raman and SHG. The maximum co-polarization Raman and cross-polarization SHG is along the crystal a-axis.

Conclusion

1. Each $PdSe_2$ crystal with a specific number of layers has its unique set of breathing mode branches with their corresponding frequencies in low frequency Raman spectroscopy, which can be used as fingerprint for unambiguous layer number determination.
2. Azimuthal angle dependent SHG and Raman were used to identify the direction of $PdSe_2$ crystalline a- and b-axis.

Reference

[1] A A Puretzky et al., *2D Mater.* 5 (2018) 035016

[2] Akinola D. Oyedele et al., *J. Am. Chem. Soc.* 2017, 139, 14090−14097